Bacteria Transport and Deposition under Unsaturated Flow Conditions: The Role of Water Content and Bacteria Surface Hydrophobicity

G. Gargiulo, S. A. Bradford,* J. Simunek, P. Ustohal, H. Vereecken, and E. Klumpp

Column experiments were conducted to investigate the transport and deposition behavior of representative hydrophobic and hydrophilic bacteria strains in sand at different water saturations. These strains are similar in surface charge, shape, and size, and differ primarily in their surface hydrophobicity and tendency to form aggregates. The amount of bacteria that were retained in the sand increased with decreasing water saturation, especially for the more hydrophobic strain that formed larger cell aggregates. Most of the cells were retained close to the column inlet, and the rate of deposition rapidly decreased with depth. The experimental data were analyzed using a mathematical model that accounted for deposition on two kinetic sites. Consideration of depth-dependent deposition in the model formulation significantly improved the description of the data, and the amount of cell retention was typically dominated by this site. The depth-dependent deposition coefficient tended to increase with decreasing water content, especially for the hydrophobic bacteria. Straining is believed to account for these observations because it increases in magnitude with increasing cell and aggregate size and when a greater fraction of the water flows through a larger number of small pore spaces with decreasing water content. Cell retention on the other kinetic deposition site was well described using a conventional model for attachment and detachment. Consistent with interaction energy calculations for bacteria attachment, however, low amounts of cell retention occurred on this site. Attempts to separately determine the amounts of attachment to solid–water and air–water interfaces were confounded by the influence of straining.

Abbreviations: DLVO, Derjaguin–Landau–Verwey–Overbeek; EC, electrical conductivity; MATH, microbial adhesion to hydrocarbon; PBS, phosphate buffer saline; TOC, total organic carbon.

ACCURATE KNOWLEDGE of the transport and fate of bacteria in subsurface environments is needed for many practical scenarios. An understanding of bacteria migration, for example, is used to assess the risk that pathogenic microorganisms pose to water resources (Ginn et al., 2002), to develop efficient water treatment methods (Tufenkji et al., 2002; Ray et al., 2002; Weiss et al., 2005), and to design bioremediation strategies for hazardous waste sites (Mishra et al., 2001; Vidali, 2001). Mobile colloids, such as bacteria, can also facilitate the transport of a wide variety of inorganic and organic contaminants that can adsorb onto these high surface area particles (Kim et al., 2003; Šimůnek et al., 2006).

Considerable research has been devoted to the fate and transport of microbes and other colloids in porous media (see reviews in Schijven and Hassanizadeh, 2000; Harvey and Harms, 2002;

G. Gargiulo, P. Ustohal, H. Vereecken, and E. Klumpp, Agrosphere (ICG-IV), Institute of Chemistry and Dynamics of the Geosphere (ICG), Forschungszentrum Jülich GmbH D-52425, Jülich, Germany; S.A. Bradford, USDA-ARS, US Salinity Lab., 450 W. Big Springs Rd., Riverside, CA 92507-4617; J. Simunek, Dep. of Environmental Sciences, Univ. of California, Riverside, CA 92521. Received 3 Apr. 2007. *Corresponding author (sbradford@ussl.ars.usda.gov).

Jin and Flury, 2002; Ginn et al., 2002; de Jonge et al., 2004). Microbe deposition in unsaturated porous media has typically been assumed to be dominated by attachment to the solid–water and/or air–water interfaces. Attachment involves mass transport of colloids to a particular interface and deposition via chemical interactions (Elimelech and O'Melia, 1990). Hence, attachment depends on the microbe's affinity for and accessibility to this interface, as well as the magnitude of the area.

Previous colloid transport studies conducted under unsaturated conditions have highlighted the role of moisture content and colloid hydrophobicity on the transport behavior (e.g., Powelson et al., 1990; Wan et al., 1994; Schaefer et al., 1998; Jewett et al., 1999; Chu et al., 2001; Sirivithayapakorn and Keller, 2003; Keller and Sirivithayapakorn, 2004; Auset et al., 2005; Crist et al., 2005; Chen and Flury, 2005). Enhanced bacteria retention has been reported for decreasing water saturation (Wan et al., 1994; Schaefer et al., 1998; Jewett et al., 1999) and has been attributed to attachment at the air–water interface, which increases in magnitude with decreasing water saturation. Bacteria hydrophobicity has also been observed to play an important role in deposition in unsaturated systems. Wan et al. (1994) and Schaefer et al. (1998) reported that for comparable experimental conditions, effluent concentrations decreased for a hydrophobic bacteria strain compared with hydrophilic bacteria. This enhanced retention of the hydrophobic bacteria has been attributed to greater attachment at the air–water interface that was controlled by long-range hydrophobic interactions.

Recent research findings, however, do not always support the concept of bacteria attachment to the air–water interface.

For example, Wan and Tokunaga (2002) demonstrated in bubble column experiments that only positively charged particles attached to the negatively charged air–water interface. Column transport experiments conducted under carefully controlled conditions of solid and/or aqueous phase chemistry have indicated that enhanced retention of colloids in unsaturated systems is unlikely to be due to attachment at the air–water interface (Chu et al., 2001; Chen and Flury, 2005).

Models of attachment to the solid–water and air–water interfaces have traditionally assumed a constant first-order deposition term, which predicts an exponential spatial distribution of retained colloids with distance (e.g., Yao et al., 1971; Logan et al., 1995; Tufenkji and Elimelech, 2004a). Under unfavorable attachment conditions (when repulsive electrostatic interactions exist between the colloids and a porous medium), however, retained colloids in saturated porous media frequently do not exhibit an exponential distribution with depth, and the deposition rate has been found to be depth dependent (Albinger et al., 1994; Baygents et al., 1998; Simoni et al., 1998; Bolster et al., 2000; DeFlaun et al., 1997; Zhang et al., 2001; Redman et al., 2001; Bradford et al., 2002, 2006b; Li et al., 2004; Bradford and Bettahar, 2005; Tong et al., 2005a,b). A variety of chemical and physical explanations have been proposed in the literature to account for these observations (Tan et al., 1994; Liu et al., 1995; Johnson and Elimelech, 1995; Kretzschmar et al., 1997; Cushing and Lawler, 1998; Bolster et al., 1999; Redman et al., 2001, 2004; Bradford et al., 2002, 2003, 2004, 2005; Tufenkji et al. 2003, 2004; Li et al. 2004, 2005; Hahn et al., 2004; Tufenkji and Elimelech, 2004b, 2005a,b; Bradford and Bettahar, 2005).

Colloid retention in porous media may occur by other processes than attachment on a single solid–water or air–water interface, which provides one plausible explanation for nonexponential deposition profiles (Bradford et al., 2002). In saturated systems, retention of colloids at two or more bounding solid–water interfaces has been referred to as *straining* (Hill, 1957; Cushing and Lawler, 1998). When multiple colloids collide and are retained in a pore constriction, this process has also been referred to as straining (Herzig et al., 1970). Other related colloid retention mechanisms may occur in unsaturated systems. *Film straining* refers to retention of colloids in thin water films that are smaller than the colloid diameter (Wan and Tokunaga, 1997), and colloids may also be retained at the solid–water–air triple point (Crist et al., 2004, 2005; Chen and Flury, 2005) in much the same way as straining at grain-to-grain contact points. Straining, film straining, and retention at the triple point share many similarities in that they all involve colloid retention at multiple interfaces and in low-velocity regions of the porous media. In this work, we use a general definition of straining as colloid retention in the smallest regions of the pore space to encompass all of these retention processes (McDowell-Boyer et al., 1986; Bradford and Torkzaban, 2008). It should be mentioned that small pore spaces such as those formed at grain–grain and solid–air–water contact points provide optimum locations for colloids that are weakly associated with the solid phase to be retained because of reduced fluid drag and size limitations (Bradford and Torkzaban, 2008).

Straining processes have only recently begun to receive research attention, and many questions have yet to be resolved. Straining processes, for example, have traditionally been assumed to be purely physical phenomena (Herzig et al., 1970; McDowell-Boyer et al., 1986) and therefore only determined by geometry considerations. Recent experimental evidence, however, indicates a strong coupling of straining processes on solution chemistry and hydrodynamics (Bradford et al., 2006a, 2007). The potential influence of colloid hydrophobicity on straining behavior has not yet been studied. Attractive hydrophobic forces between colloids, however, may result in the formation of aggregates that can subsequently be strained (Crist et al., 2005). Temporal changes in the air–water interfacial area have also been reported to produce colloid aggregates (Sirivithayapakorn and Keller, 2003). Furthermore, the average size of water-filled pores and the thickness of water films decrease with decreasing water saturation. Hence, under unsaturated conditions a greater fraction of the mobile colloids will be transported through regions of the pore space where straining processes may occur. Straining is therefore expected to increase with decreasing water saturation (Gargiulo et al., 2007).

Previous research has provided little data on bacteria retention with depth under unsaturated conditions and for different surface hydrophobicity of the bacteria. Unsaturated colloid transport studies reported in the literature also have typically not considered straining as a deposition mechanism. The objective of this research thus was to study the unsaturated transport and deposition behavior of representative hydrophilic and hydrophobic bacteria strains. For each experiment, the breakthrough curves and deposition profiles were measured. The experimental data was simulated using a two-site kinetic deposition model that accounts for time- and depth-dependent deposition processes. Fitted model parameters were used to help deduce mechanisms controlling unsaturated bacteria transport, as well as differences due to surface hydrophobicity.

Materials and Methods

Bacteria

Representative hydrophilic (*Deinococcus radiodurans*) and hydrophobic (*Rhodococcus rhodochrous*) bacterial strains in the stationary growth phase were used in the unsaturated transport experiments. *Deinococcus radiodurans* (DSMZ 20539) is a Gram-positive, nonmotile, nonspore-forming, spherical bacterium (1.0–1.5 μm diam.). It belongs to the family of *Deinococcaceae*, which includes widespread soil organisms with an extraordinary ability to survive in dry, nutrient-poor environments. This bacteria strain is known to tolerate DNA-damaging agents like ionizing radiation (Mattimore and Battista, 1996). *Rhodococcus rhodochrous* (DSMZ 11097) is a Gram-positive spherical bacterium (1 μm diam.). This strain was isolated from soil contaminated with alkenes by Kästner (1989). *Rhodococci* are aerobic, Gram-positive actinomycetes that exhibit a diverse range of metabolic activities. *Rhodococci* have the ability to degrade hydrocarbon chains and a variety of organic compounds, including xenobiotic compounds like polychlorinated biphenyls and benzothiophene. Both bacteria strains were grown on agar plates consisting of ATCC medium 220, CASO agar, peptone from casein (15.0 g), peptone from soy meal (5.0 g), NaCl (5.0 g), agar (15.0 g), and distilled water (1 L). For column experiments, both bacterial strains were cultivated at 30°C in a nutrient broth that was agitated at 13.6 rad s[−1] using a shaker. The growth media for *D. radiodurans* consisted of casein peptone, tryptic digest (10.0 g), yeast extract (5.0

g), glucose (5.0 g), NaCl (5.0 g), and distilled water (1 L). The media for *R. rhodochrous* consisted of mineral medium, Na_2HPO_4 (2.44 g), KH_2PO_4 (1.52 g), $(NH_4)_2SO_4$ (0.50 g), $MgSO_4 \times 7 H_2O$ (0.20 g), $CaCl_2 \times 2 H_2O$ (0.05 g), trace element solution (10 mL), glucose (5.0 g), and distilled water (1 L). The bacteria cells were harvested from the media in the late stationary phase by gentle centrifugation (10 min, 7100 times gravity, 25°C) and resuspended in phosphate buffer saline (PBS) 10^{-4} M, pH = 7. In this phase, the substrate had been consumed, the cell culture stopped growing, and the cells had reached a resting mode. Since no substrate was available inside the sterile sand packing, the bacteria suspension was considered to have constant properties with respect to the cell number, size, and surface properties during the experiment.

Fluorescent dyes and epifluorescent microscopy were used to visualize the bacteria cells before and after the column transport experiments and to determine the morphology of the bacteria strains. The microscope consisted of a PC-supported ECLIPSE E 1000 (Nikon, Melville, NY) with a motorized and PC–controlled three-axis cross table. The images were captured with a CCD camera (DXC-9100 P, Sony, Köln, Germany) and a Matrox Corona Framegrabber (Dorval, Quebec, Canada). The cross-table, microscope, and image acquisition were controlled by LUCIA 32 4.11 software (Nikon, Germany). Our protocol was based on that presented by Klauth et al. (2004). In brief, an aliquot of the sample was sonicated on ice for 1 min before incubation with the dye (Sybr green). The sample was pipetted into a reactor (Poschen et al., 2002) containing 4 mL of PBS (pH 7). The liquid sample was filtered through an Anodisc filter (Whatman, Kent, UK, 0.2 μm, 25-mm diam.) by applying a vacuum of 13,000 Pa, and the retained particles were washed twice with 4 mL of PBS buffer (pH 7). After washing, the filter was coated with 1.5 mL of 25 μM Sybr green solution in PBS buffer (pH 7) and incubated for 15 min. Two washing steps were subsequently performed as described above. The filter was mounted into a drop of immersion oil on a microscope slide after drying, and a drop of immersion oil was put on the surface. A cover slip was used, and an additional drop of immersion oil was put on the cover slip. The sample was viewed under blue excitation light (Nikon B-2A, excitation 450–490 nm, dichroic mirror 505 nm, longpass 520 nm) at 600-fold (in some cases, 450- or 1000-fold) magnification.

The hydrophobicity of *D. radiodurans* and *R. rhodochrous* was quantified using the microbial adhesion to hydrocarbon (MATH) approach (Rosenberg and Doyle, 1980, 1990). The test is based on the determination of the relative equilibrium-partitioning coefficient between an aqueous (polar) and a hydrocarbon (non-polar) phase (similar to the octanol-water partition coefficient for dissolved chemicals). The test was performed under the following conditions. The microbial cultures were successively harvested at different growth stages by centrifugation (7100 times gravity, 10 min. and 25°C) and resuspended in a 10^{-1} M NaCl solution. A glass test tube (10 mm diam.) was filled with 3 mL of the bacteria suspension, and the optical density of the bacteria solution was measured at 600 nm in a detector (Spectrophotometer DU800, Beckman Coulter, Fullerton, CA). Next, 300 μL of n-hexadecane was added to the suspension, and the glass tube was stirred for 2 min (Vortex-Genie 2, Bohemia, NY). When the phases in the glass tube were clearly separated, a sample of the aqueous phase was carefully taken out of the tube with a sterile glass capillary

and the sample's optical density at 600 nm was determined again. The relative hydrophobicity H_r was then calculated from

$$H_r = \left(1 - \frac{od_f}{od_i}\right) \times 100\% \qquad [1]$$

where od_i denotes the optical density of the original suspension and od_f is the optical density of equilibrated aqueous phase after partitioning. This analysis was repeated three times per sample.

Electrophoretic mobilities of the two bacteria strains were measured at 25°C using a suspension of 7×10^8 cells mL^{-1} (10^{-4} M PBS at pH = 7) using a Lazer Zee Meter (Model 501, Pen Kem, Bedford Hills, NY) equipped with a video system. The zeta potential was then calculated from the measured electrophoretic mobility using the Smoluchowski equation.

Sand

Sterile fused silica sand (Teco-Sil, C-E Minerals Greenville, TN) was used as the porous medium in the column experiments. The sand was treated with 33% peroxide to avoid any source of organic material. The grain-size distribution of this sand was determined by sieve analysis. The median grain size and the coefficient of uniformity of this sand were determined to be 567 μm and 1.87, respectively. The van Genuchten (1980) water retention curve and hydraulic conductivity function parameters were determined from multistep outflow data and inverse modeling (e.g., Hopmans et al., 2002). According to this approach, the porosity was 0.428, the saturated hydraulic conductivity was 0.576 cm min^{-1}, α (reciprocal of the air entry pressure) was 0.0234 cm^{-1}, n (related to the slope of the retention curve at the inflection point) was 12.13, and l (exponent on the tortuosity portion of the relative permeability model) was 3.617. The average pore radius of the water-filled sand was determined from the water retention curve using Laplace's equation of capillarity to be 34.7, 33.8, and 30.8 μm at water saturations of 100, 80, and 40%, respectively.

Column Experiments

Figure 1 presents a schematic of the experimental setup that was used to produce steady-state, unit gradient (i.e., identical matrix potentials at the top and bottom of the column) unsaturated flow conditions with the selected sand and bacteria (harvested in the stationary growth phase). The experimental column (8.0 cm diam.; 22.5 cm in length) was constructed from Plexiglas and consisted of four filled sections (5 cm in length) and one empty section (2.5 cm in length) that were clamped together. The bottom was formed by a porous stainless steel plate covered with a membrane (polyester fabric, mesh size 15 μm). The hydrophilic membrane was used to maintain capillary contact with the water inside the column. Before the experiments, the polyester fabric was tested to make sure that the bacteria were not retained on the membrane and that the air entry pressure was not exceeded.

The column was filled with dry sand by continuous free falling through a tube equipped with two homogenizing screens. The tube was slowly elevated during the filling procedure to keep a constant distance of 10 cm from the rising sand surface. The column was equipped with tensiometers (PMP 4070 pressure transducers, GE, Munich, Germany) near the top, in the middle, and at the bottom of the column. The tensiometers were inserted into the free gap between the sand surface and the filling tube and were embedded by the

falling sand. Because the tube had the same diameter as the column, the sand was evenly distributed over the entire cross-section of the column and resulted in compact and homogeneous packing. The porosity of the packing was determined gravimetrically (CP12001S digital balance, Sartorius, Goettingen, Germany).

At the top of the column, a sprinkling plate equipped with 80 stainless steel needles was used to distribute the influent evenly over the sand surface. The water and the solution were supplied to the sprinkling plate using a piston pump (Ismatec Reglo CPF, Ismatec Laboratoriumstechnik, Wertheim-Mondfeld, Germany; see Fig. 1). During unsaturated conditions, the air phase in the column was maintained at atmospheric pressure by means of two aeration openings. The suction at the bottom of the column was adjusted to achieve unit gradient conditions by changing the elevation of the drip point on the hanging water column. Steady-state water flow conditions were kept constant for the remainder of the transport experiment. The hydraulic properties of the homogeneous sand were assumed to be spatially invariant, and the measured capillary pressure was used as an indicator of the local water content. The total column water content was continuously monitored gravimetrically using a digital balance (CP12001S, Sartorius). The constant flow rate was measured independently using a flow meter (SF-591, softflow.de GmbH, Gross Machnow, Germany) and a digital balance, and it was fixed to a value between 165 and 170 mL h^{-1} for each experiment (a Darcy velocity of 0.055 to 0.056 cm min^{-1}).

The column bottom was connected with PVC tubes (2 mm i.d.) to a conductivity probe, UV-Vis spectrophotometer, and fluorescence detector (F1050, Merck–Hitachi, Darmstadt, Germany), as illustrated in Fig. 1. Both the bacteria and the tracer outflow concentrations were monitored on-line.

Different saturation procedures were used to generate either fully or partially saturated conditions in the column. For full water saturation (100%), the column was completely evacuated using a vacuum pump and subsequently flushed from the top with degassed buffer solution. For partial water saturation, the column containing dry sand was slowly filled at a constant flow rate supplied through the bottom. The latter procedure resulted in a water saturation (approx. 80%) containing residual entrapped air bubbles. Water saturation of 40% was obtained by gradually reducing the inflow rate at the top while at the same time as increasing the suction pressure at the bottom until unit gradient conditions were achieved. The water saturation level and the uniformity in the column were verified with the electronic balance readings and the tensiometer data at three locations. The sand in the column was then equilibrated by flushing it with several pore volumes of PBS (pH = 7, 10^{-4} M). Note that PBS may potentially modify surface charge characteristics when positive sites are present, such as on metal oxide surfaces. The PBS concentration used in the column experiments, however, was extremely low (10^{-4} M), and the sand was rigorously cleaned, so we expect this level of PBS to have a minimal impact on the bacteria transport and retention behavior.

The transport of both a conservative tracer and the bacteria cell solution was investigated by applying a continuous injection of 3.2 pore volumes to the column. Unlike the conservative tracer, the cell concentrations could not be adjusted to be identical for all the experiments but were approximately 4 to 5 × 10^7 cells mL^{-1}. The bacteria concentration in the outflow was monitored on-line every 20 s during the experiment using the UV-Vis spectrophotometer (in the range between 350 and 750 nm) and the fluorescent detector (excitation 360 nm, emission 520 nm) (Hitachi–Merck f-1050) system discussed above and a flow-through vial. Bacteria concentrations were determined from instrument response and calibration curves that were determined over relevant experimental conditions.

The conservative tracer experiment was conducted using the PBS solution as the resident and elution background solution, with demineralized water as the conservative tracer. The electrical conductivity (EC) of the column effluent was measured using a conductivity probe connected with a thermally compensated conductometer. The measured difference in EC between the PBS solution (high EC) and demineralized water (low EC) was used to quantify the transport of the demineralized water pulse.

After completion of the transport experiment, the column was rapidly frozen to avoid any water movement. To determine the bacteria retention profile, the column was unclamped and a piston was used to remove the frozen sand from the four sections. The sand from each section was partitioned into two portions (∼160 g of sand each) using a sharp knife. After the ice melted, each sample was thoroughly mixed to achieve a homogeneous concentration and was analyzed for total organic carbon (TOC) content. About 0.5 g of wet sand from each portion was used in solid-state TOC analysis (RC-412 Multiphase Determinator, Leco, St. Joseph, MI). The sand had been treated with a 33% hydrogen peroxide solution before conducting the experiments to oxidize any possible organic carbon contamination that would interfere with the TOC signal. The amount of water in the sand (difference in wet and oven dried
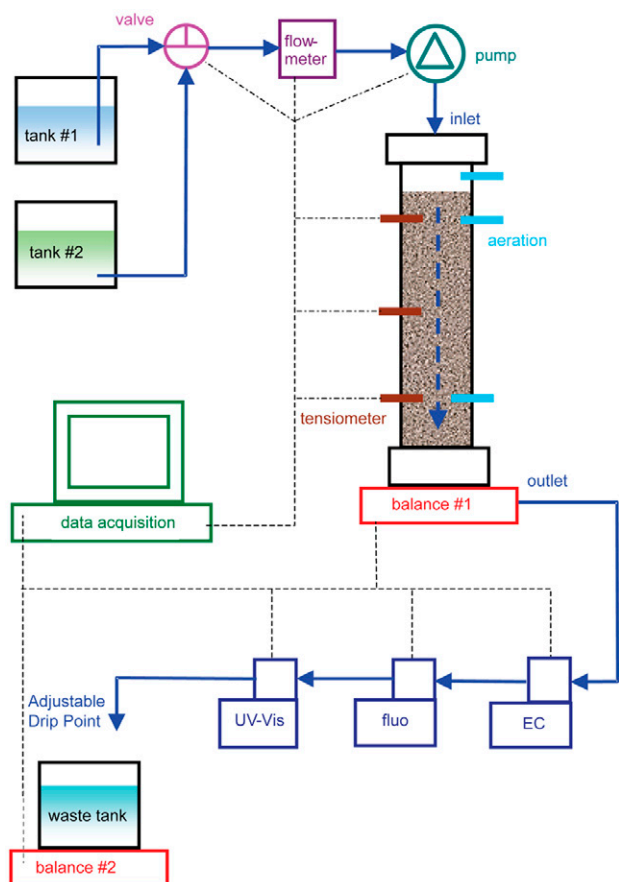

Fig. 1. Schematic of the column experiment setup.

sample) was subtracted from the total mass. The carbon concentration per gram of sand was related to the bacteria number per gram of sand using a linear calibration curve established between TOC response and step-dilutions of a bacteria solution containing known cell concentrations. The percentage of bacteria retained in the sand was calculated from the sum of the bacteria number found in each sand slice compared with the total number of bacteria injected (determined with a Coulter counter).

Theory and Model

The HYDRUS-1D code (Šimůnek et al., 2005) is a finite element model for simulating the one-dimensional movement of water, heat, and multiple solutes in variably saturated media. The code numerically solves Richards' equation for saturated–unsaturated water flow and Fickian-based advection–dispersion equations for solute transport in the liquid phase. The transport equations also include provisions for nonlinear and/or nonequilibrium reactions between the solid and liquid phases. The code may be used to analyze water and solute movement in unsaturated, partially saturated, or fully saturated porous media. The governing flow and transport equations are numerically solved using the Galerkin finite element scheme. Integration in time is achieved using implicit (backward and Crank–Nicholson) finite difference schemes. The code allows us to fit model parameters to the breakthrough curve and the retention profile simultaneously using a nonlinear least square optimization routine based on the Levenberg–Marquardt algorithm (Marquardt, 1963).

In this study, the bacteria transport was modeled using a modified form of the advection–dispersion equation that includes two kinetic deposition sites (e.g., Schijven and Simunek, 2002; Bradford et al., 2003). This approach divides the retained bacteria into two fractions ($s_1 + s_2$) and assumes different rates or processes occurring for each deposition site. The total bacteria mass balance equation is defined as

$$\frac{\partial \theta c}{\partial t} + \rho_b \frac{\partial s_1}{\partial t} + \rho_b \frac{\partial s_2}{\partial t} = \frac{\partial}{\partial x}\left(\theta D \frac{\partial c}{\partial x}\right) - \frac{\partial q c}{\partial x} \qquad [2]$$

where θ is the volumetric water content, ρ_b is the soil bulk density [M L^{-3}], t is the time [T], q is the flow rate [L T^{-1}], x is the spatial coordinate [L], D is the dispersion coefficient [L^2 T^{-1}], c is the bacteria concentration in the aqueous phase [N$_c$ L^{-3}, where N$_c$ is the number of bacteria cells], and s_1 [N$_c$ m^{-1}] and s_2 [N$_c$ m^{-1}] are the solid phase concentrations associated with deposition sites 1 and 2, respectively.

The first kinetic site (site 1) employs the conventional attachment and detachment model to describe mass transfer between the aqueous and solid phase as

$$\rho_b \frac{\partial s_1}{\partial t} = \theta \psi_t k_a c - k_d \rho_b s_1 \qquad [3]$$

where k_a is the first-order attachment coefficient [T^{-1}], k_d is the first-order detachment coefficient [T^{-1}], and ψ_t is a dimensionless colloid retention function that accounts for time-dependent deposition. To simulate reductions in the time-dependent deposition coefficient due to the blocking or filling of favorable deposition sites, ψ_t is sometimes assumed to decrease with increasing colloid mass retention. A Langmuirian dynamics (Adamczyk et al., 1994) equation has been proposed for ψ_t to describe this phenomenon as

$$\psi_t = 1 - \frac{s_1}{s_{max1}} \qquad [4]$$

in which s_{max1} is the maximum solid phase concentration [N$_c$ m^{-1}] of retained bacteria cells on site 1. Under unsaturated conditions, attachment to the solid phase and the air–water interface are lumped in the k_a term of Eq. [3].

As mentioned above, measured colloid deposition profiles are frequently not exponential with depth under unfavorable attachment conditions. A variety of physical and chemical explanations have been proposed in the literature to account for observed nonexponential deposition profiles. Unfortunately, it is frequently not possible to separate all the possible causes for this depth-dependent deposition behavior. For simplicity, the second kinetic site (site 2) lumps all depth-dependent mass transfer processes from the aqueous to the solid phase as

$$\rho_b \frac{\partial s_2}{\partial t} = \theta \psi_x k_2 c \qquad [5]$$

where k_2 [T^{-1}] is the deposition coefficient on site 2, and ψ_x is the dimensionless colloid retention function that accounts for depth-dependent deposition as

$$\psi_x = \left(\frac{d_c + x - x_0}{d_c}\right)^{-\beta} \qquad [6]$$

where d_c is the median diameter of the sand grains [L], x_0 is the coordinate [L] of the location where the depth-dependent deposition process starts (in this case, the surface of the soil profile), and β is an empirical factor controlling the shape of the spatial distribution. Bradford et al. (2003) found that a value of $\beta = 0.432$ provided an optimum description of experiments in which significant depth-dependent deposition occurred; we therefore fix β to this value in simulations discussed herein. Release of colloids from site 2 was not needed in the analysis of the data discussed below (detachment was found to play only a minor role), but is an available option in the HYDRUS-1D code.

The effluent and deposition data presented below was simulated using the HYDRUS-1D computer code (Šimůnek et al., 2005) as described by Eq. [2–6]. In these simulations, the mean pore water velocity and dispersivity were obtained by fitting the solution of the advection dispersion equation for the tracer breakthrough curve. The code allowed us to fit simultaneously the parameters k_a, k_d, k_2, and s_{max1} while considering both the breakthrough curve and the retention profile in the parameter optimization. To minimize the potential for nonunique parameter fits, we used available information to limit the number of parameters that were optimized in these simulations. Below subsequently refer to 1 site ($s_2 = 0$) model fits based on Eq. [2] and [3] with $\psi_t = 1$ and $k_d = 0$ (i.e., without blocking and detachment) as the attachment model and with $\psi_t \leq 1$ and $k_d > 0$ (i.e., with blocking of favorable deposition sites and detachment) as the Langmuirian model. Model fits based on Eq. [2–6] will be referred to as the 2 site model.

Results and Discussion

Bacteria Hydrophobicity and Morphology

The MATH test measures the hydrophobicity of bacteria as the percentage reduction of cells in the aqueous solution due to

partitioning at the hydrocarbon–water interface. The percentage hydrophobicity for the two bacteria strains was determined at various stages of the bacteria growth curve. For *R. rhodochrous*, the minimum value was 55% and the maximum was about 90%. In contrast, the percentage hydrophobicity was much lower for *D. radiodurans* and varied between 0 and 8%. The measured zeta potential for *R. rhodochrous* and *D. radiodurans* was not statistically different, with values of −47 ± 7 and −38 ± 5 mV, respectively.

Epifluorescent microscopy was a useful technique to determine the shape and morphology of the bacteria during different stages of the growth curve. Figure 2A and 2B present photographs of log phase *D. radiodurans* and *R. rhodochrous*, respectively, when suspended in 10^{-4} M PBS. The cell diameter of both *D. radiodurans* and *R. rhodochrous* is approximately 1 μm, but the photographs indicate that these cells may also form different-sized aggregates during the logarithmic growth phase. *Deinococcus radiodurans* tend to form pairs and tetra-coccus–shaped aggregates of about 2 to 4 μm in diameter, whereas *R. rhodochrous* exhibited variably sized three-dimensional aggregates that reached the size of 10 to 15 μm. Since the zeta potential for these two bacterial strains was similar, differences in the size distribution of these bacteria and cell aggregates likely occurred as a result of different factors. The bacteria surface is covered with polymers that can change with the growth phase and the availability of nutrients (Sanin et al., 2003). The bacteria surface macromolecular composition plays an important role in the cell surface hydrophobicity, adhesive properties, and in the formation of
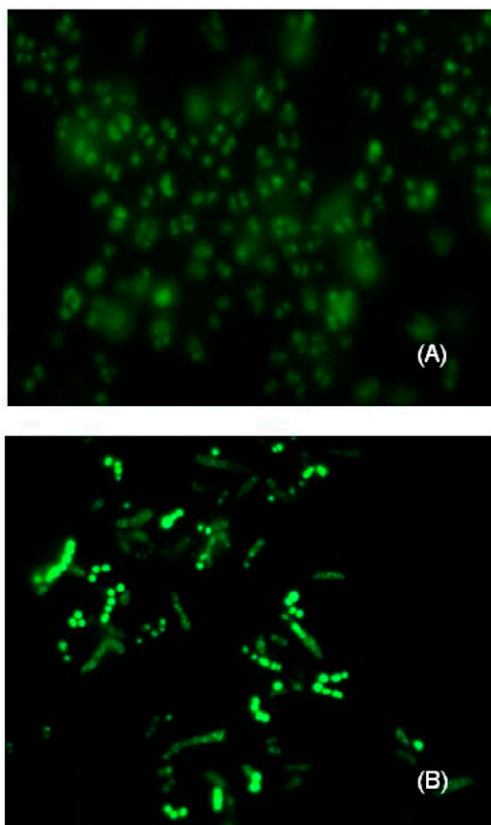
aggregates (Sanin et al., 2003; Gargiulo et al., 2007). Colloid stability and aggregation are also reported to be sensitive to the surface hydrophobicity (Crist et al., 2005; Breiner et al., 2006); that is, hydrophobic colloids are less stable than hydrophilic colloids. van Oss (1994) has proposed a mechanistic model to calculate hydrophobic interactions that is based on the Lewis acid-base free energy of adhesion. Unfortunately, disagreement about the origins of hydrophobic interactions still prevails (Tsao et al., 1993, Yaminsky and Ninham, 1993; Rabinovich and Yoon, 1994; van Oss, 1994; Yoon and Ravishankar, 1996), and quantitative theory has not been generally accepted.

For the transport experiments discussed below, the bacteria were harvested in the late stationary phase. Bacteria in the late stationary phase (also observed with the epifluorescent microscope) showed decreased aggregation behavior compared with the log phase bacteria shown in Fig. 2. Decreased hydrophobicity for bacteria in the stationary growth phase has also been observed by other researchers (van Loosdrecht et al., 1987; Fontes et al., 1991; Caccavo, 1999; Sanin et al., 2003). In the late stationary phase, *D. radiodurans* occurred primarily as single cells, whereas *R. rhodochrous* still exhibited large aggregates.

FIG. 2. Photograph of log phase (A) *Deinococcus radiodurans* and (B) *Rhodococcus rhodochrous* when suspended in 10^{-4} M phosphate buffer saline. The photographs were taken using an epifluorescent microscope.
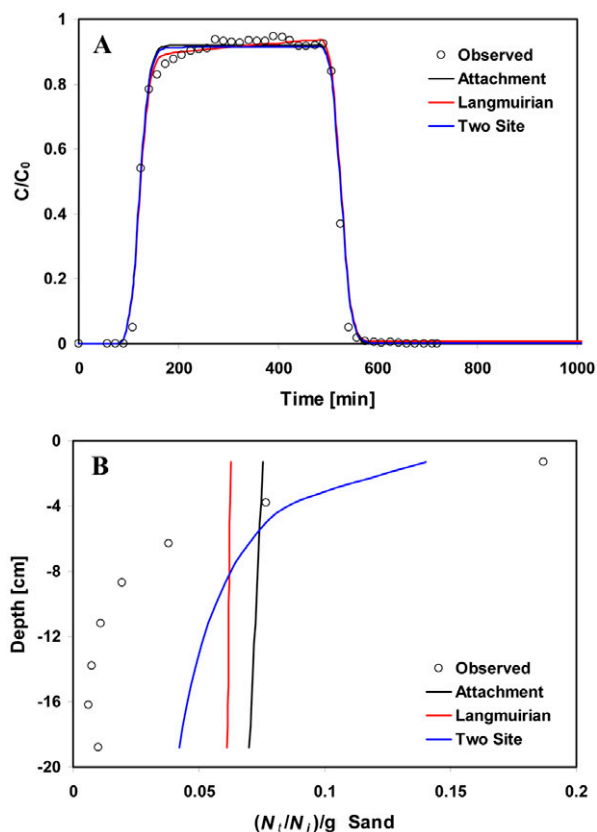
FIG. 3. (A) Measured and fitted breakthrough curves and (B) retention profiles for *Deinococcus radiodurans* at 100% saturation. Fitted curves were obtained using the attachment model, the Langmuirian model, and the 2 site model. In Fig. 3A, 127 min is equal to 1 pore volume. C/C_0 = relative effluent concentration, where C_0 is the influent concentration of bacteria; N_t, number of bacteria recovered in the sand; N_i, number in a unit volume of the input bacterial suspension.

Figures 3A, 4A, 5A and 6A, 7A, 8A present observed and simulated effluent concentration curves for stationary phase *D. radiodurans* and *R. rhodochrous*, respectively, at different water saturations (100% in Fig. 3A and 6A, 80% in Fig. 4A and 7A, and 40% in Fig. 5A and 8A). Here the relative effluent concentration, C/C_0, where C_0 is the influent concentration of bacteria, is plotted as a function of time. The corresponding observed and simulated final spatial distribution of retained bacteria after completion of the transport experiment is given in Fig. 3B, 4B, and 5B and 6B, 7B, and 8B. In this case, the data are presented as normalized concentration (number of bacteria recovered in the sand, N_t, divided by the number in a unit volume of the input bacterial suspension, N_i) per gram of dry sand and are plotted as a function of the distance from the column inlet. Table 1 gives the percentage of bacteria recovered in the effluent and deposited in the sand for these experiments. Simulations presented in Fig. 3 to 8 used the attachment, Langmuirian, and 2 site models discussed earlier. Table 2 provides a summary of the fitted attachment and Langmuirian model parameters and statistical information on the goodness-of-fit (95% confidence intervals on fitted parameters; and the coefficient of linear regression, R^2). Table 3 provides similar information for the 2 site model.

Each transport experiment was replicated twice. In general, replicate experiments exhibited consistent transport and retention behavior for given conditions (Table 1). The total mass balance for the bacteria in the transport experiments was very good, ranging from 88 to 104%. Hence, mass balance information and replicate data suggests a high level of confidence in the experimental methodologies to determine effluent and deposition data.

The mean arrival time of the bacteria breakthrough typically coincided with the conservative tracer (data not shown). The time that corresponds to 1 pore volume (dependent on the saturation, porosity, and water flow rate) is provided in the captions for Fig. 3 to 8. No appreciable retardation between the bacteria and the tracer breakthrough curves was observed. This observation was consistent for both bacteria and the different saturations. The bacteria transport, however, was clearly nonconservative because different amounts of bacteria were retained in the sand at different water contents.

Table 1 indicates that higher effluent concentrations occurred for saturated than for unsaturated systems for both bacteria strains. A reduction in the moisture content produced a decrease in the peak effluent concentration and a decrease in the total cell recovery in the effluent. For *D. radiodurans* the average percentage of bacteria recovered in the effluent was 93, 82, and 43.5% at water saturations
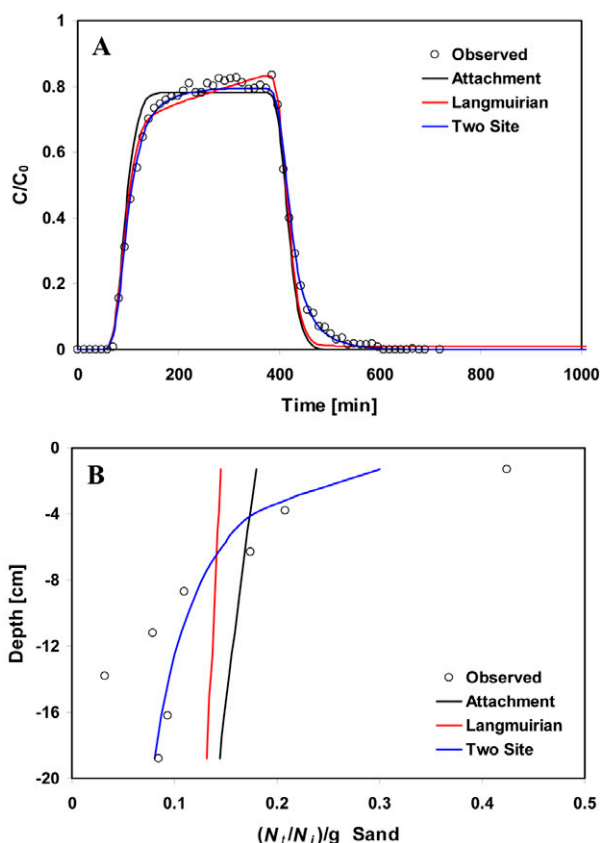

FIG. 4. (A) Measured and fitted breakthrough curves and (B) retention profiles for *Deinococcus radiodurans* at 80% saturation. Fitted curves were obtained using the attachment model, the Langmuirian model, and the 2 site model. In Fig. 4A, 101 min is equal to 1 pore volume. C/C_0 = relative effluent concentration, where C_0 is the influent concentration of bacteria; N_t, number of bacteria recovered in the sand; N_i, number in a unit volume of the input bacterial suspension.
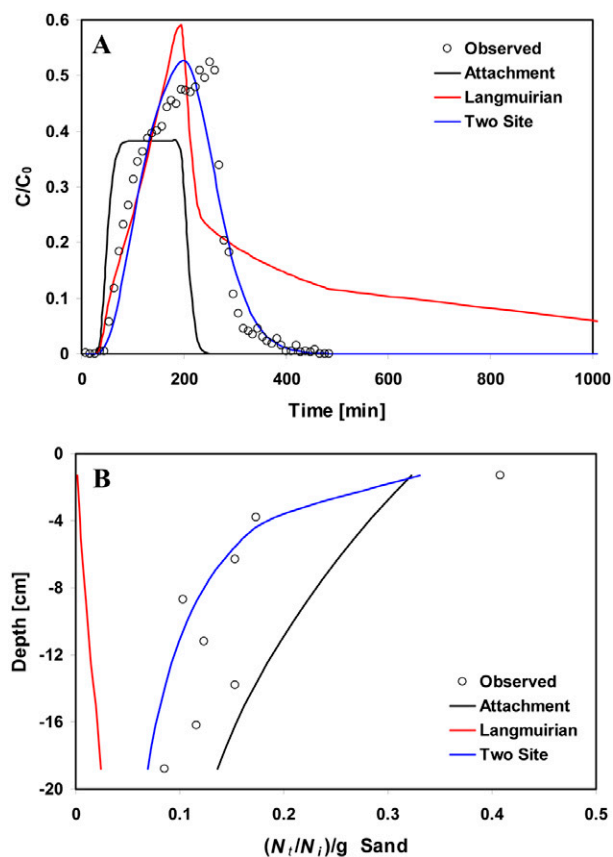

FIG. 5. (A) Measured and fitted breakthrough curves and (B) retention profiles for *Deinococcus radiodurans* at 40% saturation. Fitted curves were obtained using the attachment model, the Langmuirian model, and the 2 site model. In Fig. 5A, 55 min is equal to 1 pore volume. C/C_0 = relative effluent concentration, where C_0 is the influent concentration of bacteria; N_t, number of bacteria recovered in the sand; N_i, number in a unit volume of the input bacterial suspension.

FIG. 6. (A) Measured and fitted breakthrough curves and (B) retention profiles for *Rhodococcus rhodochrous* at 100% saturation. Fitted curves were obtained using the attachment model, the Langmuirian model, and the 2 site model. In Fig. 6A, 134 min is equal to 1 pore volume. C/C_0 = relative effluent concentration, where C_0 is the influent concentration of bacteria; N_t, number of bacteria recovered in the sand; N_i, number in a unit volume of the input bacterial suspension.
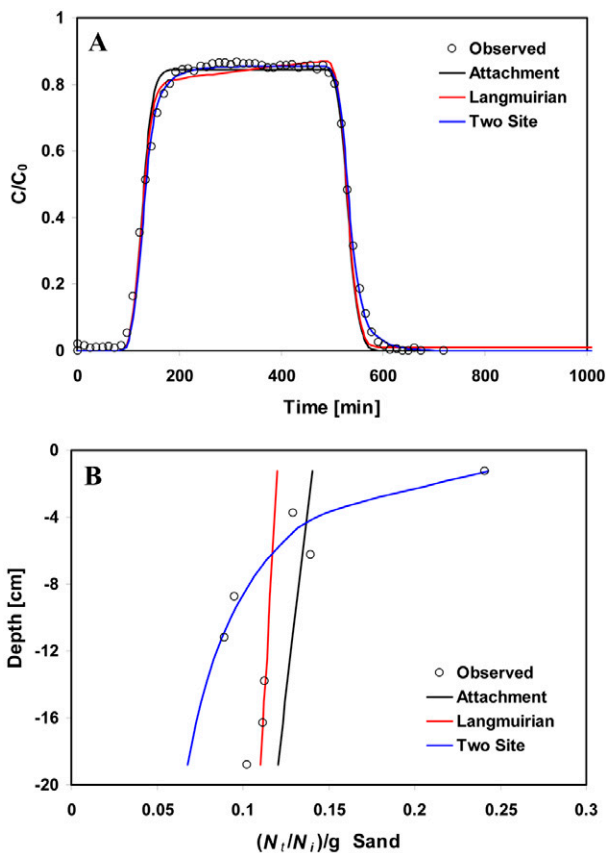

FIG. 7. (A) Measured and fitted breakthrough curves and (B) retention profiles for *Rhodococcus rhodochrous* at 80% saturation. Fitted curves were obtained using the attachment model, the Langmuirian model, and the 2 site model. In Fig. 7A, 152 min is equal to 1 pore volume. C/C_0 = relative effluent concentration, where C_0 is the influent concentration of bacteria; N_t, number of bacteria recovered in the sand; N_i, number in a unit volume of the input bacterial suspension.

of 100, 80, and 40%, respectively. Similarly, the average percentage of *R. rhodochrous* in the effluent was 82.5, 61, and 32.5% at water saturations of 100, 80, and 40%, respectively. These findings are in accordance with previously reported unsaturated bacteria transport studies (Schaefer et al., 1998; Auset et al., 2005).

The breakthrough curves at lower water saturations were more asymmetric, showing increasing effluent concentrations as the injection of bacteria proceeded. This observation suggests that the time dependency of the deposition process increased with decreasing water saturation. Time-dependent deposition has typically been ascribed to blocking of favorable attachment sites (Johnson and Elimelech, 1995; Rijnaarts et al., 1995; Schaefer et al., 1998; Bolster et al., 2001). The air–water interfacial area increases with decreasing water content (e.g., Bradford and Leij, 1997), and thus, blocking phenomena on the air–water interface should not increase with decreasing saturation. Blocking of favorable attachment sites on the solid–water interface may provide a plausible explanation of this behavior only if the accessible solid surface area to the bacteria decreases with decreasing water saturation. Alternatively, Bradford et al. (2005) and Bradford and Bettahar (2006) have suggested that filling of straining sites provides another explanation for this observation. This hypothesis is consistent with the experimental observations reported in Gargiulo et al. (2007).
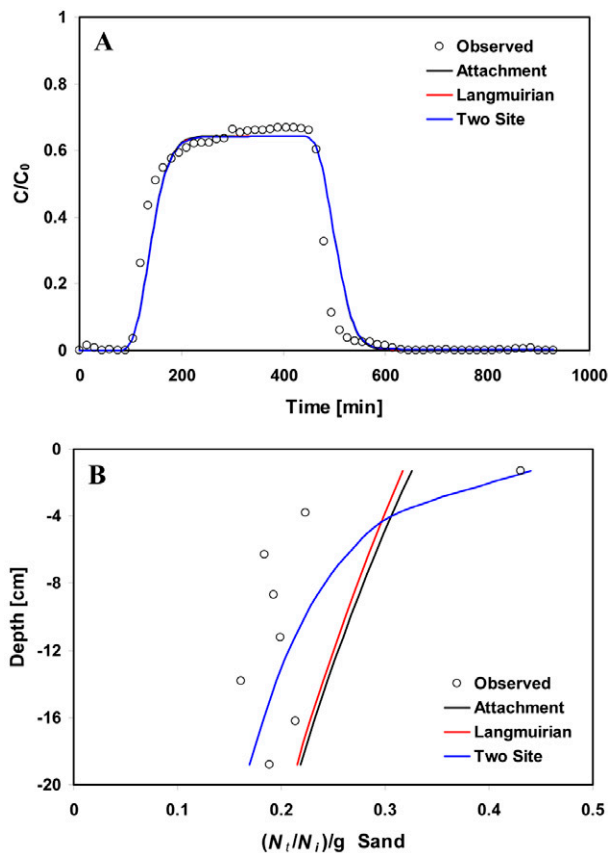
Comparisons of Fig. 3, 4, 5 with Fig. 6, 7, 8 reveal differences in the transport behavior of hydrophilic (*D. radiodurans*) and hydrophobic (*R. rhodochrous*) bacteria strains. At a given water saturation, the hydrophilic bacteria always showed higher effluent concentrations than the hydrophobic bacteria (Table 1). Differences in surface charge of the bacteria cannot explain this enhanced deposition behavior because the zeta potentials of *R. rhodochrous* and *D. radiodurans* were not statistically different (–47 ± 7 mV compared with –38 ± 5). Hence, differences in the deposition behavior are probably due to hydrophobic interactions, which enhanced the aggregation of *R. rhodochrous* (Fig. 2a and 2b). Note that there is not yet a consensus in the literature on the origins of hydrophobic interactions (Tsao et al., 1993; Yaminsky and Ninham, 1993; Rabinovich and Yoon, 1994; van Oss, 1994; Yoon and Ravishankar, 1996).

Bacteria retention inside the column was strongly influenced by the packing's water saturation. Table 1 indicates that a reduction of the water saturation tended to produce an increase in the bacteria retention. For a given water saturation, greater amounts of deposition were also observed for the more hydrophobic strain (*R. rhodochrous*) than for the hydrophilic strain (*D. radiodurans*) (Table 1).

The shape of the cell retention profile was not consistent with the first-order attachment model fit that is shown in Fig. 3B to
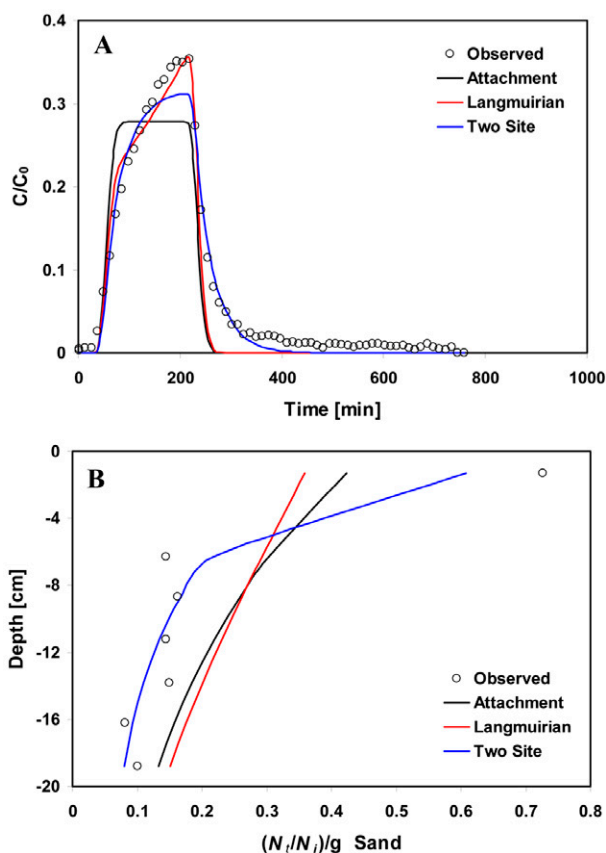
FIG. 8. (A) Measured and fitted breakthrough curves and (B) retention profiles for *Rhodococcus rhodochrous* at 40% saturation. Fitted curves were obtained using the attachment model, the Langmuirian model, and the 2 site model. In Fig. 8A, 62 min is equal to 1 pore volume. C/C_0 = relative effluent concentration, where C_0 is the influent concentration of bacteria; N_t, number of bacteria recovered in the sand; N_i, number in a unit volume of the input bacterial suspension.

8B for all saturations and for both bacteria strains (the profiles are not exponential). Compared with the attachment model fits, the observed deposition profiles typically exhibited greater retention in the section adjacent to the column inlet, especially for the drier conditions and for the strain with higher hydrophobicity (see Table 1). Consequently, the attachment model fit also overestimated the amount of bacteria retention near the column outlet. Consideration of blocking and detachment in the Langmuirian model fit to the data provided a poorer characterization of the deposition profile than the attachment model but a slightly better description of the breakthrough curves (Table 2). The coefficient of linear regression for the deposition profiles is quite poor using the attachment and Langmuirian models (Table 2). Hence, the parameter values for these models have limited physical significance and are not further discussed.

The failure of the attachment and Langmuirian models in describing colloid deposition has been reported in other experimental studies. Jewett et al. (1999) measured the deposition profile of *Pseudomonas fluorescens* in unsaturated systems. Their results indicated that the bacterial deposition rate decreased with depth and was not consistent with attachment model predictions. Deviation from the attachment model predictions was also reported by Tufenkji et al. (2003), Tufenkji and Elimelech (2004b,

2005a), and Johnson et al. (2005) in saturated column studies that used various colloids and microorganisms. These authors attributed nonexponential deposition profiles to surface heterogeneity of colloids and/or porous media, and attachment in the secondary energy minima of the Derjaguin–Landau–Verwey–Overbeek (DLVO) potential energy profile. Conversely, Bradford et al. (2002, 2003) attributed deviations from attachment model predictions to straining of colloids in the smallest regions of the pore space.

Additional simulations were conducted to better quantify mechanisms of bacteria deposition using the 2 site model. Similar to Bradford et al. (2003), we assumed in this analysis that depth-dependent deposition processes (site 2) occur primarily near the column inlet and that conventional attachment (site 1 with $\psi_t = 1$) dominates in the region of the deposition profile that exhibits less concentration change with distance; in this case, for depths greater than ~6 cm from the inlet. Figures 3 through 8 and Tables 2 and 3 indicate that the 2 site model provided a significantly better description of experimental data than either the attachment or the Langmuirian models, especially the deposition profiles. This improvement was not due to differences in the number of fitting parameters, as both the 2 site and the Langmuirian models had three parameters that were optimized.

Table 4 provides the corresponding mass balance information for deposition on sites 1 and 2 that were determined in HYDRUS. The depth-dependent deposition (site 2) accounts for 71 to 99% and 51 to 97% of the total deposition for *D. radiodurans* and *R. rhodochrous*, respectively. The total amount of the bacteria deposited in site 2 also dramatically increased with decreasing water saturation. This was especially true for the hydrophobic bacteria *R. rhodochrous* that forms larger aggregates and had as much as 97% retained in site 2 at a water saturation of 40%. These findings are consistent with trends in site 2 model parameters with saturation and bacteria hydrophobicity (Table 3). The values of k_2 for both *D. radiodurans* and *R. rhodochrous* increased with decreasing water saturation. At a given saturation, the value of k_2 for the hydrophobic *R. rhodochrous* was always higher than that for the hydrophilic *D. radiodurans*.

We believe that straining of cells and/or aggregates can explain the observed trends discussed above for k_2. Straining of colloids has been reported to occur when the ratio of the colloid to the median grain diameter is greater than 0.003 to 0.005 (Bradford et al., 2003; Bradford and Bettahar, 2006; Bradford et al., 2006c), with increasing amounts of deposition occurring for larger values of this ratio. This finding has also been confirmed in pore-scale micromodel studies using latex microspheres (Bradford et al., 2005) and bacteria (Bradford et al., 2006a,b). On the basis

TABLE 1. Percentage of bacteria in the outflow and retained in the column for two replicates (1 and 2).

Replicate	Saturation	*Rhodococcus rhodochrous*		*Deinococcus radiodurans*	
		Outflow	Retained	Outflow	Retained
			%		
1	100	86	8 (3)[†]	95	6 (4)[†]
2	100	79	12	91	4
1	80	63	33 (12)[†]	88	14 (7)[†]
2	80	59	35	76	16
1	40	36	65 (31)[†]	47	53 (23)[†]
2	40	29	75	40	48

[†] Retained in the top 0 to 5 cm of the column.

TABLE 2. Fitted parameters of the first-order attachment and Langmuirian models for *Deinococcus radiodurans* and *Rhodococcus rhodochrous*.

Parameter[†]	Saturation 100% Value	95% CI[‡]	Saturation 80% Value	95% CI	Saturation 40% Value	95% CI
First-order attachment model (*D. radiodurans*)						
k_a (min⁻¹)	6.90e-04	± 5.09e+00	2.54e-03	± 6.51e+00	1.85e-02	± 1.40e+01
R^2	0.992		0.974		0.298	
R^2 (BTC)§	0.994		0.985		0.315	
R^2 (RP)¶	0.633		0.673		0.599	
Langmuirian blocking model (*D. radiodurans*)						
k_a (min⁻¹)	9.94e-04	± 3.67e-04	3.87e-03	± 6.97e-04	4.36e-02	± 1.68e-02
k_d (min⁻¹)	2.00e-04	± 4.13e-04	1.72e-04	± 2.08e-04	4.29e-03	± 2.08e-03
s_{max1} (N_t/N_i)/g sand	1.71e-01	± 1.80e-01	3.06e-01	± 1.11e-01	3.56e-01	± 1.54e-01
R^2	0.993		0.980		0.518	
R^2 (BTC)	0.995		0.992		0.643	
R^2 (RP)	0.600		0.627		0.430	
First-order attachment model (*R. rhodochrous*)						
k_a (min⁻¹)	1.31e-03	± 4.99e+01	3.05e-03	± 1.10e+01	2.20e-02	± 7.98e-00
R^2	0.991		0.950		0.826	
R^2 (BTC)	0.993		0.958		0.909	
R^2 (RP)	0.485		0.421		0.734	
Langmuirian blocking model (*R. rhodochrous*)						
k_a (min⁻¹)	1.73e-03	± 3.58e-04	3.08e-03	± 6.09e-04	2.68e-02	± 4.70e-03
k_d (min⁻¹)	1.53e-04	± 1.88e-04	2.96e-05	± 1.63e-04	1.00e-06#	± 2.42e-04
s_{max1} (N_t/N_i)/g sand	3.62e+01	± 2.01e-01	1.00e+03#	± 1.33e+06	6.48e-01	± 3.27e-01
R^2	0.993		0.950		0.830	
R^2 (BTC)	0.995		0.957		0.969	
R^2 (RP)	0.461		0.419		0.627	

† k_a, first-order attachment coefficient; k_d, first-order detachment coefficient; s_{max1}, maximum solid phase concentration of retained bacteria cells; N_t, number of bacteria recovered in the sand; N_i, number in a unit volume of the input bacterial suspension.
‡ CI, confidence interval.
§ BTC, breakthrough curve.
¶ RP, retention profile.
# Upper or lower constraint.

TABLE 3. Fitted parameters of the two site depth-dependent deposition model for *Deinococcus radiodurans* and *Rhodococcus rhodochrous*.

Parameter[†]	Saturation 100% Value	95% CI[‡]	Saturation 80% Value	95% CI	Saturation 40% Value	95% CI
Deinococcus radiodurans						
k_a (min⁻¹)	5.11e-05	± 3.17e-04	3.46e-03	± 1.70e-03	9.77e-02	± 4.27e-02
k_d (min⁻¹)	2.41e-03	± 3.90e-02	2.81e-02	± 1.62e-02	7.70e-02	± 3.55e-02
k_2 (min⁻¹)	0.0051	± 0.0023	0.0172	± 9.33e-04	0.078	± 0.0087
β	0.432		0.432		0.432	
R^2	0.994		0.996		0.928	
R^2 (BTC)§	0.994		0.998		0.931	
R^2 (RP)¶	0.980		0.954		0.896	
Rhodococcus rhodochrous						
k_a (min⁻¹)	1.88e-03	± 6.43e-04	1.55e-03	± 1.25e-04	1.58e-02#	± 6.47e-03
k_d (min⁻¹)	3.38e-02	± 1.38e-02	6.36e-05	± 3.15e-04	4.00e-02	± 1.99e-03
k_2 (min⁻¹)	0.00892	± 0.00044	0.011	± 0.0088	0.144	± 0.0060
β	0.432		0.432		0.432	
R^2	0.998		0.955		0.977	
R^2 (BTC)	0.998		0.958		0.987	
R^2 (RP)	0.869		0.771		0.960	

† k_a, first-order attachment coefficient; k_d, first-order detachment coefficient; β, empirical factor controlling the shape of the spatial distribution.
‡CI, confidence interval.
§ BTC, breakthrough curve.
¶ RP, retention profile.
# Upper or lower constraint.

of the cell size and aggregation behavior presented in Fig. 2, the ratio of the cell aggregate size to median sand size is expected to range from 0.002 to 0.007 for *D. radiodurans* and from 0.002 to 0.026 for *R. rhodochrous*. Hence, straining is anticipated to occur for both bacteria strains in this sand, but greater amounts of straining are expected for the more hydrophobic bacteria (*R. rhodochrous*) that produced larger cell aggregates (see Fig. 2). The retention of aggregates by straining is also in accordance with the pore-scale observations of Sirivithayapakorn and Keller (2003) and Crist et al. (2004).

The observed dependency of k_2 on water saturation can also be explained by straining. Figure 9 presents an illustration of a triangular-shaped capillary tube under saturated and unsaturated conditions. Potential straining sites are indicated in this figure where multiple interfaces intersect (at the air–water–solid triple point and at vertices of the triangular capillary tube). For a given water flow rate through the capillary tube, a greater fraction of the water flow will occur near straining sites under unsaturated than under saturated conditions. Furthermore, the number of straining sites will increase under unsaturated conditions due to the presence of more air–water–solid triple points. Both of these factors are expected to contribute to greater amounts of straining (higher values of k_2) with decreasing water saturation.

The relative water flux to straining sites as a function of the water saturation can be estimated from measured capillary pressure-saturation curve information using the approach outlined by Bradford et al. (2006a). In brief, a hypothetical fraction of the pore space where straining occurs (γ) is assumed or estimated for a particular porous medium and colloid-size distribution. Measured capillary pressure-saturation data is then used in a pore-size distribution model (Burdine, 1953) to estimate a water relative permeability for the fraction of the pore space that is defined by γ. The water flux to this region is subsequently calculated using Darcy's law in conjunction with this relative permeability information. For the sand used in our study, Fig. 10 presents an illustrative plot of the relative water flux to straining sites as a function of water saturation for various hypothetical values of γ. The relative water flux to straining sites increases dramatically when the saturation decreases or γ increases. For our particular sand and bacteria, the value of γ will be appropriately equal to the residual water saturation (e.g., <10%).

It unlikely that surface heterogeneity of the bacteria and sand can account for the large amounts of bacteria retention in site 2 that increased with decreasing water saturation, for the following reasons. First, DLVO calculations following the approach outlined by Bradford et al. (2006a) indicate highly unfavorable conditions for attachment to the solid–water interface (primary or secondary minimum of the interaction energy profile) for the selected solution and solid chemistries, cell aggregate sizes, and the measured ranges in cell zeta potential. Second, DLVO calculations presented by Crist et al. (2005) also indicate a low potential for attachment of the bacteria and cell aggregates to the air–water interface (due to repulsive

Saturation	Total mass injected	Mass Site 1	Mass Site 2	Mass Site 1	Mass Site 2
%		cells cm^{-2}		%	
		Deinococcus radiodurans			
100	4.56E+09	4.56E+07	3.99E+08	0.01 ± 5.6	8.74 ± 6.01
80	8.41E+08	9.58E+06	1.68E+08	1.14 ± 0.39	20.4 ± 0.93
40	1.69E+08	2.65E+07	6.71E+07	15.7 ± 7.9	39.7 ± 1.21
		Rhodococcus rhodochrous			
100	1.07E+09	3.85E+06	1.54E+08	0.36 ± 0.13	14.4 ± 0.65
80	2.89E+08	5.03E+07	5.32E+07	17.4 ± 8.6	18.4 ± 10.3
40	4.30E+08	9.72E+06	2.89E+08	2.26 ± 1.16	67.4 ± 0.88

van der Waals and electrostatic interactions). Third, attachment of *D. radiodurans* on the air–water interface is unlikely to occur by hydrophobic interactions because this bacterium had a low hydrophobicity (MATH was 0–8%). Hence, the large amounts of *D. radiodurans* retention that increased with decreasing water saturation cannot be explained by attachment to the air–water interface (Table 1).

Table 4 indicates that the total attachment (site 1) to solid–water and air–water interfaces only accounted for 0.7 to 16.7% of the injected bacteria cells into a column. These low percentages are likely to be more physically realistic for attachment than the amounts of retention on site 2 given the findings of the DLVO calculations discussed in the proceeding paragraph. The fitted attachment coefficient k_a in Table 3 is a lumped parameter that characterizes both the attachment to the solid surface and to the air–water interface. Due to the confounding influence of straining in site 2 and the relatively low amounts of bacteria retention in site 1, it may not be possible to mechanistically separate the influence of attachment to the solid–water and air–water interfaces.

Hence, below, we only discuss general trends in site 1 parameters. Mass balance information for sites 1 and 2 that was calculated in HYDRUS is also discussed and is presented in Table 4.

For *D. radiodurans*, the value of k_a increased with decreasing water saturation, suggesting greater attachment. Consistent with these findings, the information in Table 4 indicates that a greater percentage of *D. radiodurans* cells was retained on site 1 with decreasing water saturation (at water saturations of 100, 80, and 40%, the retained mass on site 1 was 0.01, 1.14, and 15.7%, respectively). The value of k_d for *D. radiodurans* also increased with decreasing water saturation and was greater than or of a similar magnitude as k_a. These observations indicate that attachment was approaching linear equilibrium sorption conditions (van Genuchten et al., 1974).

Conversely, values of k_a and k_d for *R. rhodochrous* at different water saturations did not follow a systematic trend, and mass balance information for site 1 (Table 4) indicates that cell retention actually decreased with decreasing water saturation. This result is somewhat misleading; it is really a consequence of straining of aggregates of this bacterium. Equation [3] indicates that the amount of attachment is proportional to the aqueous phase concentration of the cells. When deposition on site 2 increases, the aqueous concentration of the cells is decreased, and the rate of attachment on site 1 will therefore also decrease.

Under saturated conditions, the value of k_a for *D. radiodurans* was lower than that for *R. rhodochrous*. This result is consistent with the higher hydrophobicity showed by *R. rhodochrous* compared with *D. radiodurans* and suggests that *R. rhodochrous* has a higher sticking coefficient (assuming that the single collector contact efficiency is the same for both strains). Cell surface hydrophobicity has been reported to directly influence bacteria adhesion behavior (Rijnaarts et al., 1995; van Loosdrecht et al., 1987). A similar conclusion about bacteria adhesion and hydrophobicity was reported by Unc and Goss (2003), who found slower attachment and detachment rates for hydrophilic compared with hydrophobic strains under saturated conditions.

Conclusions

The aim of this work was to study the transport and deposition behavior of representative hydrophilic and hydrophobic
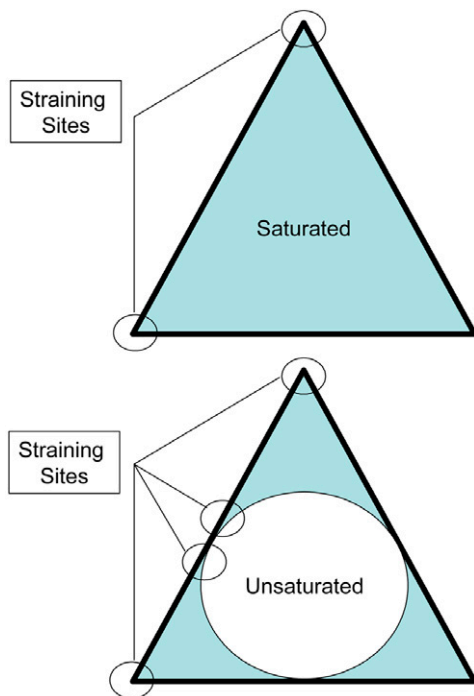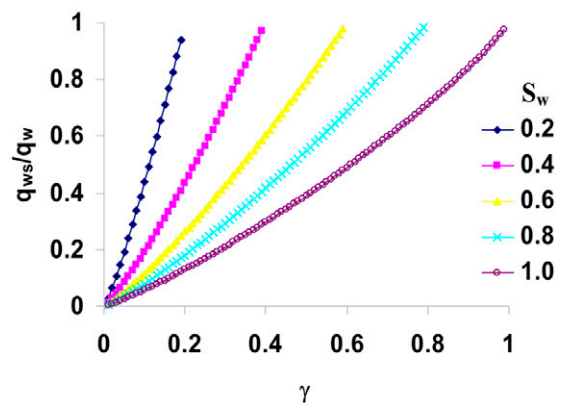

FIG. 9. Illustration of a triangular-shaped capillary tube under saturated and unsaturated conditions. Potential straining sites are indicated in this figure where multiple interfaces intersect (at the air–water–solid triple point and the vertices of the triangular capillary tube).

FIG. 10. A plot of the relative water flux to straining sites (q_{ws}/q_w; where q_{ws} and q_w are the Darcy water velocities to straining sites and the porous medium at a given water saturation, respectively) for various hypothetical fractions of the pore space where straining occurs (γ) and the indicated water saturations (S_w).

bacteria strains under unsaturated conditions. Two bacteria strains, *Deinococcus radiodurans* and *Rhodococcus rhodochrous*, that were used in the transport experiments strongly differed in hydrophobicity but are similar in size (1 μm), surface charge, and shape (coccoid). Although both strains were observed to form aggregates in solution, the hydrophobic *R. rhodochrous* tended to form larger aggregates (as large as 10–15 μm).

For both bacteria strains, a decrease in water content led to decreasing effluent concentrations and increased retention of the bacteria. This effect was more pronounced for the hydrophobic strain and with drier conditions. The profiles of retained cells were not exponential with depth. Most of the bacteria were deposited in the first centimeters below the column inlet and the profile monotonically decreased with increasing depth.

Three models were used to characterize the bacteria transport and retention data: a first-order attachment model, a Langmuirian (attachment, detachment, and blocking) model, and a 2 site (attachment, detachment, and depth-dependent deposition) model. In contrast to attachment or Langmuirian models, the 2 site model accurately simulated the experimental breakthrough curves and deposition data for all the saturations and for both bacteria strains. The vast majority of the deposited cells were retained in site 2 that considered depth–dependent deposition. Analysis of the transport and retention data and fitted model parameters suggests that straining was the dominant mechanism of cell retention on site 2. Specifically, straining is expected to increase with increasing hydrophobicity of the bacteria because of the tendency of these bacteria to form larger aggregates than the hydrophilic bacteria. Furthermore, straining is expected to increase with decreasing water saturation because a greater fraction of the water flows through a larger number of small pore spaces (near grain to grain contacts and air-water-solid triple points). Conversely, DLVO calculations suggest that attachment to the solid–water and air–water interfaces cannot likely account for the observed magnitudes of depth-dependent deposition on site 2 but rather was consistent with relatively low amounts of attachment on site 1. It was not possible to mechanistically separate the influence of attachment to the solid–water and air–water interfaces due to the confounding influence of straining.

References

Adamczyk, Z., B. Siwek, M. Zembala, and P. Belouschek. 1994. Kinetics of localized adsorption of colloid particles. Adv. Colloid Int. Sci. 48:151–280.

Albinger, O., B.K. Biesemeyer, R.G. Arnold, and B.E. Logan. 1994. Effect of bacterial heterogeneity on adhesion to uniform collectors by monoclonal populations. FEMS Microbiol. Lett. 124:321–326.

Auset, M., A.A. Keller, F. Brissaud, and V. Lazarova. 2005. Intermittent filtration of bacteria and colloids at pore and column scales. Water Resour. Res. 41(9):W09408, doi:10.1029/2004WR003611.

Baygents, J.C., J.R. Glynn, Jr., O. Albinger, B.K. Biesemeyer, K.L. Ogden, and R.G. Arnold. 1998. Variation of surface charge density in monoclonal bacterial populations: Implications for transport through porous media. Environ. Sci. Technol. 32:1596–1603.

Bolster, C.H., A.L. Mills, G.M. Hornberger, and J.S. Herman. 1999. Spatial distribution of deposited bacteria following miscible displacement experiments in intact cores. Water Resour. Res. 35:1797–1807.

Bolster, C.H., A.L. Mills, G. Hornberger, and J. Herman. 2000. Effect of intra-population variability on the long-distance transport of bacteria. Ground Water 38:370–375.

Bolster, C.H., A.L. Mills, G.M. Hornberger, and J.S. Herman. 2001. Effect of surface coatings, grain size, and ionic strength on the maximum attainable coverage of bacteria on sand surfaces. J. Contam. Hydrol. 50:287–305.

Bradford, S.A., and M. Bettahar. 2005. Straining, attachment, and detachment of Cryptosporidium oocysts in saturated porous media. J. Environ. Qual. 34:469–478.

Bradford, S.A., and M. Bettahar. 2006. Concentration dependent colloid transport in saturated porous media. J. Contam. Hydrol. 82:99–117.

Bradford, S.A., M. Bettahar, J. Simunek, and M.Th. van Genuchten. 2004. Straining and attachment of colloids in physically heterogeneous porous media. Vadose Zone J. 3:384–394.

Bradford, S.A., and F.J. Leij. 1997. Estimating interfacial areas for multi-fluid soil systems. J. Contam. Hydrol. 27:83–105.

Bradford, S.A., J. Simunek, M. Bettahar, Y.F. Tadassa, M.Th. van Genuchten, and S.R. Yates. 2005. Straining of colloids at textural interfaces. Water Resour. Res. 41:W10404, doi:10.1029/2004WR003675.

Bradford, S.A., J. Simunek, M. Bettahar, M.Th. van Genuchten, and S.R. Yates. 2003. Modeling colloid attachment, straining and exclusion in saturated porous media. Environ. Sci. Technol. 37:2242–2250.

Bradford, S.A., J. Šimůnek, M. Bettahar, M.Th. van Genuchten, and S.R. Yates. 2006a. Significance of straining in colloid deposition: Evidence and implications. Water Resour. Res. 42:W12S15, doi:10.1029/2005WR004791.

Bradford, S.A., J. Simunek, and S.L. Walker. 2006b. Transport and straining of *E. coli* O157:H7 in saturated porous media. Water Resour. Res. 42:W12S12, doi:10.1029/2005WR4805.

Bradford, S.A., Y.F. Tadassa, and Y. Pachepsky. 2006c. Transport of *Giardia* and manure suspensions in saturated porous media. J. Environ. Qual. 35:749–757.

Bradford, S.A., and S. Torkzaban. 2008. Colloid transport and retention in unsaturated porous media: A review of interface, collector, and pore scale processes and models. Vadose Zone J. (in press).

Bradford, S.A., S. Torkzaban, and S.L. Walker. 2007. Coupling of physical and chemical mechanisms of colloid straining in saturated porous media. Water Res. 41:3012–3024.

Bradford, S.A., S.R. Yates, M. Bettahar, and J. Simunek. 2002. Physical factors affecting the transport and fate of colloids in saturated porous media. Water Resour. Res. 38(12):1327, doi:10.1029/2002WR001340.

Breiner, J.M., M.A. Anderson, H.W.K. Tom, and R.C. Graham. 2006. Properties of surface-modified colloidal particles. Clays Clay Miner. 54:12–24.

Burdine, N.T. 1953. Relative permeability calculations from pore size distribution data. Trans. Am. Inst. Miner. Metall. Petrol. Eng. 198:71–78.

Caccavo, F., Jr. 1999. Protein-mediated adhesion of the dissimilatory Fe (III)-reducing bacterium Shewanella alga BrY to hydrous ferric oxide. Appl. Environ. Microbiol. 65:5017–5022.

Chen, G., and M. Flury. 2005. Retention of mineral colloids in unsaturated porous media as related to their surface properties. Coll. Surf. Physicochem. Eng. Aspects 256:207–216.

Chu, Y., Y. Jin, M. Flury, and M.V. Yates. 2001. Mechanisms of virus removal during transport in unsaturated porous media. Water Resour. Res. 37:253–263.

Crist, J.T., J.F. McCarthy, Y. Zevi, P. Baveye, J.A. Throop, and T.S. Steenhuis. 2004. Pore-scale visualization of colloid transport and retention in partly saturated porous media. Vadose Zone J. 3:444–450.

Crist, J.T., Y. Zevi, J.F. McCarthy, J.A. Throop, and T.S. Steenhuis. 2005. Transport and retention mechanisms of colloids in partially saturated porous media. Vadose Zone J. 4:184–195.

Cushing, R.S., and D.F. Lawler. 1998. Depth filtration: Fundamental investigation through three-dimensional trajectory analysis. Environ. Sci. Technol. 32:3793–3801.

DeFlaun, M.F., C.J. Murray, M. Holben, T. Scheibe, A. Mills, T. Ginn, T. Griffin, E. Majer, and J.L. Wilson. 1997. Preliminary observations on bacterial transport in a coastal plain aquifer. FEMS Microbiol. Rev. 20:473–487.

de Jonge, L.W., C. Kjaergaard, and P. Moldrup. 2004. Colloids and colloid-facilitated transport of contaminants in soils: An introduction. Vadose Zone J. 3:321–325.

Elimelech, M., and C.R. O'Melia. 1990. Kinetics of deposition of colloidal particles in porous media. Environ. Sci. Technol. 24:1528–1536.

Fontes, D.E., A.L. Mills, G.M. Hornberger, and J.S. Herman. 1991. Physical and chemical factors influencing transport of microorganisms through porous media. Appl. Environ. Microbiol. 57:2473–2481.

Gargiulo, G., S.A. Bradford, J. Simunek, P. Ustohal, H. Vereecken, and E. Klumpp. 2007. Bacteria transport and deposition under unsaturated conditions: The role of matrix grain size and the bacteria surface protein. J. Contam. Hydrol. 92:255–273.

Ginn, T.R., B.D. Wood, K.E. Nelson, T.D. Scheibe, E.M. Murphy, and T.P. Clement. 2002. Processes in microbial transport in the natural subsurface. Adv. Water Resour. 25:1017–1042.

Hahn, M.W., D. Abadzic, and C.R. O'Melia. 2004. Aquasols: On the role of secondary minima. Environ. Sci. Technol. 38:5915–5924.

Harvey, J.W., and H. Harms. 2002. Tracers in groundwater: Use of microorganisms and microspheres. p. 3194–3202. In G. Britton (ed.) Encyclopedia of environmental microbiology. John Wiley & Sons, New York.

Herzig, J.P., D.M. Leclerc, and P. LeGoff. 1970. Flow of suspension through porous media: Application to deep filtration. Ind. Eng. Chem. 62:129–157.

Hill, W.A. 1957. An analysis of sand filtration. J. Sanitary Eng. Div. 83(SA3):1276-1–1276-9.

Hopmans, J.W., J. Šimůnek, N. Romano, and W. Durner. 2002. Inverse modeling of transient water flow. p. 963–1008. In J.H. Dane and G.C. Topp (ed.) Methods of soil analysis: Part 1, Physical methods. 3rd ed. SSSA, Madison, WI.

Jewett, D.G., B.E. Logan, R.G. Arnold, and R.C. Bales. 1999. Transport of Pseudomonas fluorescens strain P17 through quartz sand columns as a function of water content. J. Contam. Hydrol. 36:73–89.

Jin, Y., and M. Flury. 2002. Fate and transport of viruses in porous media. Adv. Agron. 77:39–102.

Johnson, P.R., and M. Elimelech. 1995. Dynamics of colloid deposition in porous media: Blocking based on random sequential adsorption. Langmuir 11:801–812.

Johnson, W.P., M. Tong, and X. Li. 2005. Colloid deposition in environmental porous media: Deviation from existing theory is the norm; not the exception. Eos Trans AGU 86(18):179–180.

Kästner, M. 1989. Anreicherung und Isolierung von Chlorkohlenwasserstoffe abbauenden Mikroorganismen unter verschiedenen physiologischen Bedingungen- Abbaukinetiken und Test auf technische Nutzbarkeit zur Sanierung kontaminierter Grundwässer. Ph.D. diss., Technischen Universität Braunschweig.

Keller, A.A., and S. Sirivithayapakorn. 2004. Transport of colloids in unsaturated porous media: Explaining large scale behavior based on pore scale mechanisms. Water Resour. Res. 40:W12403, doi:10.1029/2004WR003315.

Kim, S.B., M.Y. Corapcioglu, and D.J. Kim. 2003. Effect of dissolved organic matter and bacteria on contaminant transport in riverbank filtration. J. Contam. Hydrol. 66:1–23.

Klauth, P., R. Wilhelm, E. Klumpp, L. Poschen, and J. Groeneweg. 2004. Enumeration of soil bacteria with the green fluorescent nucleic acid dye Sytox green in the presence of soil particles. J. Microbiol. Methods 59:189–198.

Kretzschmar, R., K. Barmettler, D. Grolimun, Y.D. Yan, M. Borkovec, and H. Sticher. 1997. Experimental determination of colloid deposition rates and collision efficiencies in natural porous media. Water Resour. Res. 33:1129–1137.

Li, X., T.D. Scheibe, and W.P. Johnson. 2004. Apparent decreases in colloid deposition rate coefficient with distance of transport under unfavorable deposition conditions: A general phenomenon. Environ. Sci. Technol. 38:5616–5625.

Li, X., P. Zhang, C.L. Lin, and W.P. Johnson. 2005. Role of hydrodynamic drag on microsphere deposition and re-entrainment in porous media under unfavorable conditions. Environ. Sci. Technol. 39:4012–4020.

Liu, D., P.R. Johnson, and M. Elimelech. 1995. Colloid deposition dynamics in flow-through porous media: Role of electrolyte concentration. Environ. Sci. Technol. 29:2963–2973.

Logan, B.E., D.G. Jewett, R.G. Arnold, E.J. Bouwer, and C.R. O'Melia. 1995. Clarification of clean-bed filtration models. J. Environ. Eng. 121:869–873.

Marquardt, D.W. 1963. An algorithm for least-squares estimation of nonlinear parameters. SIAM J. Appl. Math. 11:431–441.

Mattimore, V., and J.R. Battista. 1996. Radioresistance of Deinococcus radiodurans: Functions necessary to survive ionizing radiation are also necessary to survive prolonged desiccation. J. Bacteriol. 178:633–637.

McDowell-Boyer, L.M., J.R. Hunt, and N. Sitar. 1986. Particle transport through porous media. Water Resour. Res. 22:1901–1921.

Mishra, S., J. Jeevan, C.K. Ramesh, and L. Banwari. 2001. In situ bioremediation potential of an oily sludge-degrading bacterial consortium. Curr. Microbiol. 43:328–335.

Poschen, L., P. Klauth, J. Groeneweg, and R. Wilhelm. 2002. A filtration, incubation and staining reactor including a new protocol for FISH. J. Microbiol. Methods 50:97–100.

Powelson, D.K., J.R. Simpson, and C.P. Gerba. 1990. Virus transport and survival in saturated and unsaturated flow through soil columns. J. Environ. Qual. 19:396–401.

Rabinovich, Ya.I., and R.-H. Yoon. 1994. Use of atomic force microscope for the measurements of hydrophobic forces between silanated silica plate and glass sphere. Langmuir 10:1903–1909.

Ray, C., T.W. Soong, Y.Q. Lian, and G.S. Roadcap. 2002. Effect of flood-induced chemical load on filtrate quality at bank filtration sites. J. Hydrol. 266:235–258.

Redman, J.A., S.B. Grant, T.M. Olson, and M.K. Estes. 2001. Pathogen filtration, heterogeneity, and the potable reuse of wastewater. Environ. Sci. Technol. 35:1798–1805.

Redman, J.A., S.L. Walker, and M. Elimelech. 2004. Bacterial adhesion and transport in porous media: Role of the secondary energy minimum. Environ. Sci. Technol. 38:1777–1785.

Rijnaarts, H.H.M., W. Norde, E.J. Bouwer, J. Lyklema, and A.J.B. Zehnder. 1995. Reversibility and mechanism of bacterial adhesion. Coll. Surf. Biointerfaces 4:1–63.

Rosenberg, M., and R.J. Doyle. 1980. Adherence of bacteria to hydrocarbon. FEMS Microbiol. Lett. 9:29–33.

Rosenberg, M., and R.J. Doyle. 1990. Microbial cell surface hydrophobicity: History, measurement, and significance. p. 1–37. In R.J. Doyle and M. Rosenberg (ed.) Microbial cell surface hydrophobicity. American Soc. for Microbiology, Washington, DC.

Sanin, S.L., F.D. Sanin, and J.D. Bryers. 2003. Effect of starvation on the adhesive properties of xenobiotic degrading bacteria. Process Biochem. 38:909–914.

Schaefer, A., P. Ustohal, H. Harms, F. Stauffer, T. Dracos, and A.J.B. Zehnder. 1998. Transport of bacteria in unsaturated porous media. J. Contam. Hydrol. 33:149–169.

Schijven, J.F., and S.M. Hassanizadeh. 2000. Removal of viruses by soil passage: Overview of modeling, processes and parameters. Crit. Rev. Environ. Sci. Technol. 30:49–127.

Schijven, J.F., and J. Simunek. 2002. Kinetic modeling of virus transport at the field scale. J. Contam. Hydrol. 55:113–135.

Simoni, S.F., H. Harms, T.N.P. Bosma, and A.J.B. Zehnder. 1998. Population heterogeneity affects transport of bacteria through sand columns at low flow rates. Environ. Sci. Technol. 32:2100–2105.

Šimůnek, J., M.Th. van Genuchten, and M. Šejna. 2005. The HYDRUS-1D software package for simulating the one-dimensional movement of water, heat, and multiple solutes in variably-saturated media: Version 3.0, HYDRUS Software Series 1. Dep. of Environmental Sciences, Univ. of California-Riverside, Riverside.

Šimůnek, J., C. He, J.L. Pang, and S.A. Bradford. 2006. Colloid-facilitated transport in variably saturated porous media: Numerical model and experimental verification. Vadose Zone J. 5:1035–1047.

Sirivithayapakorn, S., and A.A. Keller. 2003. Transport of colloids in unsaturated porous media: A pore scale observation of processes during the dissolution of air–water interface. Water Resour. Res. 39(12):1346, doi:10.1029/2003WR002487.

Tan, Y., J.T. Cannon, P. Baveye, and M. Alexander. 1994. Transport of bacteria in an aquifer sand: Experiments and model simulations. Water Resour. Res. 30:3243–3252.

Tong, M., T.A. Camesano, and W.P. Johnson. 2005a. Spatial variation in deposition rate coefficients of an adhesion-deficient bacterial strain in quartz sand. Environ. Sci. Technol. 39:3679–3687.

Tong, M., X. Li, C.N. Brow, and W.P. Johnson. 2005b. Detachment-influenced transport of an adhension-deficient bacterial strain within water-reactive porous media. Environ. Sci. Technol. 39:2500–2508.

Tsao, Y.H., D.F. Evans, and H. Wennerstrom. 1993. Long-range attraction between a hydrophobic surface and a polar surface is stronger than that between two hydrophobic surfaces. Langmuir 9:779–785.

Tufenkji, N., and M. Elimelech. 2004a. Correlation equation for predicting single-collector efficiency in physiochemical filtration in saturated porous media. Environ. Sci. Technol. 38:529–536.

Tufenkji, N., and M. Elimelech. 2004b. Deviation from the classical colloid filtration theory in the presence of repulsive DLVO interactions. Langmuir 20:10818–10828.

Tufenkji, N., and M. Elimelech. 2005a. Breakdown of colloid filtration theory: Role of secondary energy minimum and surface charge heterogeneities. Langmuir 21:841–852.

Tufenkji, N., and M. Elimelech. 2005b. Spatial distributions of *Cryptosporidium* oocysts in porous media: Evidence for dual mode deposition. Environ. Sci. Technol. 39:3620–3629.

Tufenkji, N., G.F. Miller, J.N. Ryan, R.W. Harvey, and M. Elimelech. 2004. Transport of *Cryptosporidium* oocysts in porous media: Role of straining and physicochemical filtration. Environ. Sci. Technol. 38:5932–5938.

Tufenkji, N., J.A. Redman, and M. Elimelech. 2003. Interpreting deposition patterns of microbial particles in laboratory-scale column experiments. Environ. Sci. Technol. 37:616–623.

Tufenkji, N., J.N. Ryan, and M. Elimelech. 2002. The promise of bank filtration. Environ. Sci. Technol. 36:422a–428a.

Unc, A., and M.J. Goss. 2003. Movement of faecal bacteria through the vadose zone. Water Air Soil Pollut. 149:327–337.

Vidali, M. 2001. Bioremediation: An overview. Pure Appl. Chem. 73:1163–1172.

van Genuchten, M.Th. 1980. A closed-form equation for predicting the hydraulic conductivity of unsaturated soils. Soil Sci. Soc. Am. J. 44:892–898.

van Genuchten, M.Th., J.M. Davidson, and P.J. Wierenga. 1974. An evaluation of kinetic and equilibrium equations for the prediction of pesticide movement through porous media. Soil Sci. Soc. Am. J. 38:29–35.

van Loosdrecht, M.C.M., J. Lyklema, W. Norde, G. Schraa, and A.J.B. Zehnder. 1987. The role of bacterial cell wall hydrophobicity in cell attachment. Appl. Environ. Microbiol. 53:1893–1897.

van Oss, C.J. 1994. Interfacial forces in aqueous media. Marcel Dekker, New York.

Wan, J., and T.K. Tokunaga. 1997. Film straining of colloids in unsaturated porous media: Conceptual model and experimental testing. Environ. Sci. Technol. 31:2413–2420.

Wan, J., J.L. Wilson, and T.L. Kieft. 1994. Influence of the gas water interface on transport of microorganisms through unsaturated porous media. Appl. Environ. Microbiol. 60:509–516.

Wan, J.M., and T.K. Tokunaga. 2002. Partitioning of clay colloids at air–water interfaces. J. Colloid Interface Sci. 247:54–61.

Weiss, W.J., E.J. Bouwer, R. Aboytes, M.W. LeChevallier, C.R. O'Melia, B.T. Le, and K.J. Schwab. 2005. River filtration for control of microorganisms results from field monitoring. Water Res. 39:1990–2001.

Yaminsky, V.V., and B.W. Ninham. 1993. Hydrophobic force: Lateral enhancement of subcritical fluctuations. Langmuir 9:3618–3624.

Yao, K.M., M.T. Habibian, and C.R. O'Melia. 1971. Water and waste water filtration: Concepts and applications. Environ. Sci. Technol. 5:1105–1112.

Yoon, R.-H., and S.A. Ravishankar. 1996. Long-range hydrophobic forces between mica surfaces in alkaline dodecylammonium chloride solutions. J. Coll. Interf. Sci. 179:403–411.

Zhang, P., W.P. Johnson, T.D. Scheibe, K. Choi, F.C. Dobbs, and B.J. Mailloux. 2001. Extended tailing of bacteria following breakthrough at the Narrow Channel Focus Area, Oyster, Virginia. Water Resour. Res. 37:2687–2698.